ELSEVIER

International Journal of Mass Spectrometry 184 (1999) 217–231

International Journal of Mass Spectrometry

Metastable decay of molecular fragment ions sputtered from hydrocarbon polymers under keV ion bombardment

A. Delcorte*, P. Bertrand

Université Catholique de Louvain, PCPM, Croix du Sud 1, B-1348 Louvain-la-Neuve, Belgium

Received 12 November 1998; accepted 2 January 1999

Abstract

To investigate the metastable decay processes for molecular ions sputtered from hydrocarbon polymers with different degrees of unsaturation, polyisobutylene, polybutadiene, and polystyrene thin films were bombarded by 15 keV, Ga^+ ions and the secondary ions were mass and energy analyzed by means of a time-of-flight spectrometer. In general, the kinetic energy distributions show that an important fraction of the secondary ions is detected with an energy deficit, due to the dissociation of their metastable parents in the linear part of the spectrometer. The analysis of the energy spectra leads to propose two types of metastable decay reactions: fast, unindentified dissociation in the acceleration section of the spectrometer and delayed H and H_2 losses in the drift section of the spectrometer. The interpretation of the results in the frame of the unimolecular reactions theory indicates that the decay rates of these reactions are in the range 10^7–10^8 s^{-1} (fast decay) and 10^4–10^5 s^{-1} (H and H_2 loss), which corresponds to half lives of 10 ns to 0.1 μs and 10 to 100 μs, respectively. On average, the fraction of ions produced in the vacuum increases with the mass of the daughter ions. When comparing the three polymers, the metastable decay for the lowest mass range ($0 < m/z < 100$) is increasing when decreasing unsaturation (polyisobutylene > polybutadiene > polystyrene). The important analytical issue of these unimolecular decomposition reactions is addressed, too. (Int J Mass Spectrom 184 (1999) 217–231) © 1999 Elsevier Science B.V.

Keywords: Secondary ion mass spectrometry; Sputtering; Ion emission; Unimolecular reactions; Metastable ions; Polystyrene; Polyisobutylene; Polybutadiene

1. Introduction

The bombardment of solid surfaces by keV [1–3] and MeV [4] primary ions leads to the sputtering of molecular fragment ions or clusters. During the emission process, the departing species receive both kinetic and internal energy, the latter being shared between the different vibration and rotation modes [5,6]. If the polyatomic particle lays prior to emission in a region close to the primary impact point, where the deposited energy is high, the internal energy excess will probably cause its direct fragmentation [7–10]. On the other hand, if the received energy is lower, the internal energy may be absorbed in the rotation and vibration modes without fragmentation, resulting in the emission of the particle in an excited state. These excited molecular ions may then decompose during their time-of-flight in the spectrometer, which has important fundamental and analytical implications [11–13].

Following the unimolecular reaction theory [14], the metastable decay of a parent ion can be described

* Corresponding author. E-mail: delcorte@pcpm.ucl.ac.be

Presented at the 1st European Workshop on Secondary Ion Mass Spectrometry, Münster, 4–6 October 1998.

PII S1387-3806(99)00012-3

with a simple exponential equation. The constant appearing in the exponential is defined as the rate of dissociation (r) and the half live of the metastable ion population ($\tau_{1/2}$) is proportional to the inverse of the rate r. The parameter governing the rate of dissociation of excited species is the excess of internal energy (E_{int}) in the particle. In the frame of ion-induced particle desorption, metastable decay processes have been investigated by several authors for organic [11–13,15–21] and inorganic samples [15,21–26], using keV [11–12,15–20,22–26] and MeV [13,19–21] primary ions. In these works, the nature and importance of the metastable decay processes and, in several cases, the decay rates and lifetimes of the parent ions have been studied.

With our time-of-flight secondary ion mass spectrometry (TOF-SIMS), the daughter ions resulting from unimolecular dissociation of their metastable parents in the linear part of the spectrometer can be observed in the energy spectra of the secondary ions [12,18]. Indeed, when they dissociate, the parents share their kinetic energy between the neutral and ion fragments in a proportion depending on the respective masses of these fragments. Consequently, the daughter ions originating from the dissociation process will be detected with a kinetic energy $E_{\text{acc}} - \Delta E_{\text{neutral}}$, lower than the kinetic energy of identical ions directly emitted from the surface [25,26].

For short lifetimes, typically in the range 10^{-9}–10^{-7} s, the dissociation reaction occurs in the acceleration section of the TOF spectrometer. Then, the metastable ions decompose before being completely accelerated (3 kV). These daughter ions having a kinetic energy deficit constitute a “negative energy” tail in the kinetic energy distributions (KEDs). In principle, the simultaneous knowledge of the negative part of the KED and of the mass of the neutral fragment allows one to deduce the lifetime of such metastable ions [25,26].

For longer lifetimes, approximately 10^{-6}–10^{-4} s, the parent ions decompose in the field-free drift section of the spectrometer preceding the first electrostatic analyzer. In this case, the daughter ions of a given reaction have the same kinetic energy deficit, which is independent of the dissociation time because they are no longer accelerated in this section. Thus, they constitute a well-defined peak in the energy spectrum, and the mass of the neutral lost can be easily determined knowing the energy deficit [12].

In previous papers, the unimolecular dissociation of metastable molecular ions has been observed for dibenzanthracene and polystyrene [18], and for more complicated polymers containing nitrogen [12]. It was observed that some ions containing aromatic rings present a bimodal structure in these KEDs, which was explained by the loss of hydrogen from larger parent ions in the linear part of the spectrometer. The KEDs of parent ions and metal–cationised molecules of triacontane and tetraphenylnaphtalene indicated an important contribution of fast metastable decay reactions, too [27]. In addition, preliminary results concerning the fast metastable decay of fragment ions sputtered from polyisobutylene and polystyrene have been reported recently [28].

In the following, we report on the extensive study of metastable decay reactions in the case of molecular fragment ions sputtered from hydrocarbon polymers with various degrees of unsaturation: polyisobutylene (PIB), polybutadiene (PBD), and polystyrene (PS). This work extends our previous studies [18,28] in several ways: three different hydrocarbon polymers are compared; the metastable decay in the acceleration section and in the field-free drift region are clearly distinguished and investigated separately; the results are modeled on the basis of the unimolecular reactions theory. The discussion will be mainly focused on three important issues: (1) the metastable decay reactions and their analytical consequences; (2) the exact nature and relative importance of the decay channels for the three studied polymers; (3) the estimated decay rates and lifetimes for the different kinds of reactions.

2. Experimental

2.1. Samples

Monodisperse PS $[–CH_2–CH(C_6H_5)–]_n$ was received from the University of Liège (M_n = 60 000). PIB $[–CH_2–C(CH_3)_2–]_n$ and PBD $[–CH_2–CH{=}CH–$

$CH_2–]_n$ were purchased from Aldrich Chemie (high molecular weight). All the polymers were dissolved in toluene (from 0.05 to 5 mg/mL). They were prepared as thin films cast on silicon substrates (0.25 cm^2), by depositing a droplet of the solution on the substrate. Prior to deposition, the substrates were rinsed in water of HPLC grade from a milli-Q system (Millipore), isopropanol, and hexane. The low concentration of the solutions allowed us to deposit very thin polymer layers, ensuring a good electric contact between the top surface and the sample holder. To verify this, all the energy measurements were done with samples for which the substrate secondary ion peaks were present in the TOF-SIMS spectra.

2.2. SIMS analyses

The secondary ion mass analyses and the KED measurements were performed in a PHI-EVANS Time-of-Flight SIMS (TRIFT 1) using a (5 kHz) pulsed Ga^+ beam (15 kV, 400–800 pA dc) [29]. The angle between the gallium source and the spectrometer axis (perpendicular to the surface) is 35°. In order to avoid polymer degradation [30], the primary beam was rastered onto a (130 × 130 μm^2) area, allowing to keep the ion fluence below 5×10^{11} ions/cm^2 for one spectrum. For a KED measurement, ~20 spectra were recorded on the same sample area with different energy windows and the total ion fluence was kept below 10^{13} ions/cm^2.

During the secondary ion extraction periods, a (3000-Δ) V potential is applied to the sample where Δ is adjustable in order to acquire a selected window of the KED and this 3 kV corresponds to the nominal extraction voltage. The departing secondary ions are accelerated between the sample and the extraction plate (grounded entrance of the first Einzel lens) and focused before to enter a field-free drift region. They are afterwards 270° deflected by three hemispherical electrostatic analyzers (ESAs) before reaching the detector. At the crossover following the first ESA (at 90° with respect to the spectrometer axis), they are energy selected by a slit of fixed width (100 μm corresponding to a passband of 1.5 eV). The acquisition of mass spectra for different sample voltages allows the collection of a complete KED, a 1 V increase of the sample potential corresponding to a 1 eV decrease in the KED. An alternative way to measure the KED is to keep the sample voltage at the fixed nominal value (3 kV) and to shift the energy slit perpendicularly to the beam in order to accept different regions of the KED. The spatial distribution is then converted into an energy distribution owing to an empirical equation derived from the simulation of the ion trajectories [31]. The zero of energy scale is estimated in the following from the intersection between the tangent to the increasing part of the KED of the atomic substrate ions (Si^+) and the energy axis. The corrected value of the sample voltage, giving the initial kinetic energy of the secondary ions, will be called "apparent kinetic energy" in the following.

For the integral KED measurement, the external edge of the energy slit is used to cut the high energy part of the distributions. In this way, the measured signal is the integral of the low energy part of the KED, including ions with a kinetic energy deficit. To vary the upper limit of the integral, several acquisitions are realised with different sample voltages.

3. Theoretical considerations

According to the theory of unimolecular reactions [14], for a given reaction, the number of metastable parents Y_p in time t is given by

$$Y_p(t) = Y^0 \exp(-rt) \quad (1)$$

where Y^0 is the initial number of parent ions and r is the dissociation rate, depending on the internal energy of the fragment. The number of daughter ions in time t can be easily obtained from

$$Y_d(t) = Y^0 - Y_p(t) \quad (2)$$

and its time derivative can be calculated by

$$\frac{dY_d}{dt} = rY^0 \exp(-rt) \quad (3)$$

In the following, the use of these simple equations to describe the metastable ions distributions will imply

two severe hypotheses: (1) the decay of the considered parent occurs mainly via a single reaction, and not by several parallel reaction channels; (2) the internal energy distribution of the parent ion is narrow and centered around a value E_{int} corresponding to a given rate r.

3.1. Unimolecular dissociation in the acceleration section

For an ion of mass m losing a neutral of mass Δm in the acceleration section of the spectrometer, the relation between the energy deficit ΔE_k and the time-of-flight t needed to reach the dissociation point is described by

$$t = \frac{ml_{acc}}{eV}\left(\frac{2}{\Delta m}\right)^{1/2}\Delta E_k^{1/2} \tag{4}$$

where e is the electron charge, l_{acc} is the length of the acceleration section, and V is the accelerating voltage. Thus, the increment of energy $d\Delta E_k$ corresponds to an increment of time

$$dt = \frac{1}{2}\frac{ml_{acc}}{eV}\left(\frac{2}{\Delta m}\right)^{1/2}\Delta E_k^{-1/2}d\Delta E_k$$

$$= \frac{1}{2}K\Delta E_k^{-1/2}d\Delta E_k \tag{5}$$

where

$$K = \frac{ml_{acc}}{eV}\left(\frac{2}{\Delta m}\right)^{1/2}$$

With these equivalences, one can calculate the derivative of the number of daughter ions as a function of the energy deficit ΔE_k

$$\frac{dY_d}{d\Delta E_k} = \frac{dY_d}{dt}\frac{dt}{d\Delta E_k}$$

$$= \frac{1}{2}KrY^0\Delta E_k^{-1/2}\exp(-rK\Delta E_k^{1/2})$$

$$= -Y^0\frac{d}{d\Delta E_k}\exp(-rK\Delta E_k^{1/2}) \tag{6}$$

It will be shown in the results part that the quantity $dY_d/d\Delta E_k$ is directly obtained from the kinetic energy distribution of the ion. In addition, the integral of the daughter ion intensity will be available from a slightly different experiment (see sec. 2). Following our formalism and Eq. (6), this integral is given by

$$\int_{\Delta E_k}^{\infty} dY_d = Y^0\exp(-rK\Delta E_k^{1/2}) \tag{7}$$

3.2. Unimolecular dissociation in the drift section

In the case of hydrogen loss reactions, the KED will allow us to determine the number of daughter ions formed in the field-free drift section of the spectrometer [12,18]. Assuming the same hypotheses as before, this value can be calculated from

$$Y_d^{drift} = \int_{t_1}^{t_2} dY_d$$

$$= -Y^0\exp(-rt_1)\{\exp[-r(t_2-t_1)]-1\} \tag{8}$$

obtained by integration of Eq. (3). In Eq. (8), Y_d^{drift} is the number of daughters formed in the drift section, and t_1 is the time spent by the parent in the acceleration section, and t_2 is the time-of-flight of the parent when reaching the entrance of the first hemispherical electrostatic analyser. t_1 is deduced from the equation of ion motion in the electric field of the acceleration section. Replacing t_1 and t_2 by their value gives

$$Y_d^{drift} = -Y^0\exp\left(-r\sqrt{2\frac{ml_{acc}^2}{eV}}\right)$$

$$\times\left[\exp\left(-r\sqrt{\frac{ml_{drift}^2}{2eV}}\right)-1\right] \tag{9}$$

where l_{drift} is the length of the field-free drift section. Due to the unimolecular dissociation process, the number of detected parent ions (Y_p^{det}) will be equal to

$$Y_p^{\text{det}} = Y^0 \exp\left\{-\mathrm{r}\sqrt{\frac{\mathrm{m}}{\mathrm{eV}}\left[2\mathrm{l}_{\mathrm{acc}}^2 + \frac{1}{2}(l_{\mathrm{tot}} - l_{\mathrm{acc}})^2\right]}\right\} \approx Y^0 \exp\left(-r\sqrt{\frac{ml_{\mathrm{tot}}^2}{2eV}}\right) \quad (10)$$

where l_{tot} is the total length of spectrometer. The simplification in the last term of Eq. (10) is justified by the fact that $l_{\mathrm{tot}} \cong 1000 \times l_{\mathrm{acc}}$. With this equation, Y^0 can be calculated, and the integral Y_d^{drift} can be rewritten as

$$Y_d^{\mathrm{drift}} = Y_p^{\mathrm{det}} \exp\left(r\sqrt{\frac{ml_{\mathrm{tot}}^2}{2eV}}\right) \exp\left(-\mathrm{r}\sqrt{2\frac{\mathrm{ml}_{\mathrm{acc}}^2}{eV}}\right) \cdot \left[1 - \exp\left(-\mathrm{r}\sqrt{\frac{\mathrm{ml}_{\mathrm{drift}}^2}{2eV}}\right)\right] \quad (11)$$

As the quantities Y_d^{drift} and Y_p^{det} may be deduced from the KED measurement, Eq. (11) will allow us to calculate the value of r for the decay reactions observed in the drift section of the spectrometer.

4. Results and discussion

4.1. Molecular ion yields

The positive secondary ion mass spectra of PIB, PBD, and PS are displayed in Fig. 1. These polymers have been extensively studied in the past and their mass spectra have been published and discussed elsewhere (PIB [28,30,32–33], PBD [32–34], and PS [34,35]). Our spectra are in good agreement with the literature. These polymer surfaces may be distinguished on the basis of the fingerprint region of the positive mass spectra ($0 \leq m/z \leq 200$). Briefly, the characteristic peaks of PIB correspond to $C_xH_{2x\pm1}$ ions ($C_4H_7^+$—$m/z = 55$, $C_4H_9^+$—$m/z = 57$, $C_6H_{11}^+$—$m/z = 83$, $C_7H_{13}^+$—$m/z = 97$), whereas the unsaturated fingerprint ions of PS are closer to the formula C_xH_x ($C_3H_3^+$—$m/z = 39$, $C_4H_3^+$—$m/z = 51$, $C_6H_5^+$—$m/z = 77$, $C_7H_7^+$—$m/z = 91$). PBD

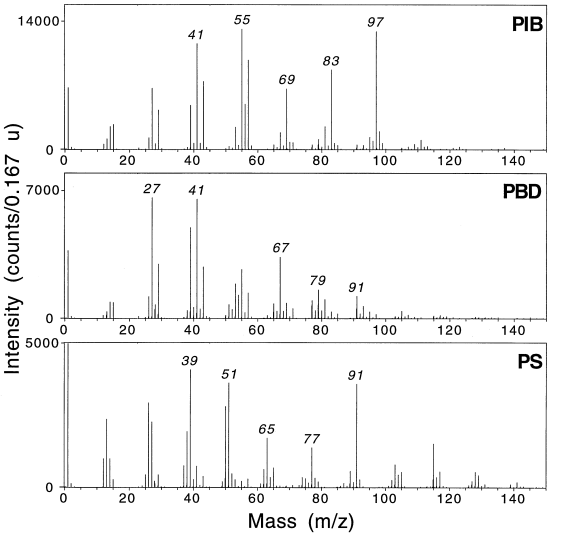

Fig. 1. Positive secondary ion mass spectra of PIB, PBD, and PS.

exhibits molecular ions of intermediate hydrogen content ($C_3H_5^+$—$m/z = 41$, $C_5H_7^+$—$m/z = 67$, $C_6H_7^+$—$m/z = 79$). Due to the fact that these polymers are constituted of carbon and hydrogen only, the spectra can be easily interpreted.

For this study, three solutions of PIB were realized with concentrations of approximately 0.05, 0.5, and 5 mg/mL. Fig. 2 shows the intensity variation of two characteristic ions sputtered from samples cast from these solutions. The organic ion intensities are reported as a function of the silicon Si^+ intensity, which gives an idea about the layer homogeneity and compacity. The variation observed between different areas of samples realised with the same solution indicates that the samples are not homogeneous. Nevertheless, a continuous line can be drawn through the three sets of experiments, suggesting that the intensities are mainly influenced by the variation of the coverage density. With increasing silicon intensity, the characteristic PIB ion intensities first increase to a maximum, showing an important enhancement due to the presence of the substrate. This substrate effect has been observed for PS cast on silver, too [18]. Beyond the maximum, the intensity of $C_6H_{11}^+$ and $C_7H_{13}^+$ decreases quickly, indicating that the uncovered surface fraction becomes more and more important. Fig.

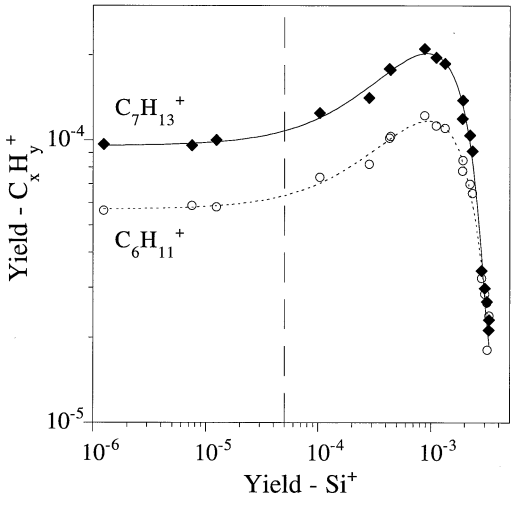

Fig. 2. Correlation between the useful secondary ion yield *[number of detected secondary ions per primary ion]* of two characteristic ions of PIB and the yield of the substrate ion, Si^+, for dilute PIB solutions cast on silicon.

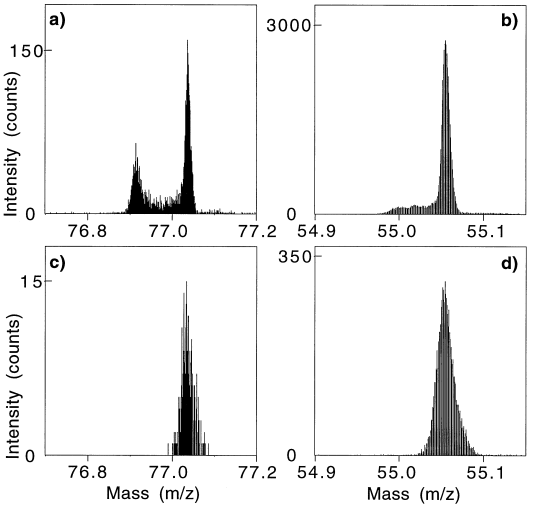

Fig. 3. Partial positive secondary ion mass spectra of PIB showing $C_6H_5^+$ and $C_4H_7^+$ peaks, (a) and (b): usual tuning of the spectrometer; (c) and (d): with energy slit centered around 2 eV.

2 shows that the influence of the substrate becomes predominent for $Y(\mathrm{Si}) > 10^{-4}$. In this region, the development of the collision cascades in the heavier silicon support may modify the sputtering mechanisms for the organic adsorbates. In addition, the ionization probability is probably enhanced by the presence of oxygen at the surface (native silicon oxide). Therefore, the intensity of the silicon signal will be systematically verified in the following in order to remain in the "thick layer" regime for the KED measurements.

4.2. Metastable decay reactions

Despite the simplicity of the hydrocarbon polymer formulae, several peaks in the mass spectra cannot be identified with the peak assessment procedure. Based on an adequate mass calibration of the spectra, this routine of the Cadence 1 software (Charles Evans & Assoc.) calculates cluster ion masses based on the combination of a number of atoms of different elements. The proposed combinations and the mass deviation with respect to the centroid of the unknown peaks in the mass spectrum are listed, leading to a fast determination of the observed ion compositions. In general, this routine is very efficient, provided that an accurate mass calibration on reference peaks has been realised prior to identification. However, for the studied hydrocarbons, although the main peaks of the spectrum may be easily recognised, in agreement with the literature, many secondary peaks or intense tails do not correspond to any possible combination. These are observed mostly below $m/z = 100$ for PIB and PBD. Unknown peaks appear as satellites of aromatic or unsaturated ion peaks (C_6H_5, C_7H_7) [Fig. 3(a)]. In addition, most of the other peaks in the spectra are asymetric, with a more or less pronounced, intriguing low-mass tail [Fig. 3(b)]. The use of an energy slit, accepting ions with a kinetic energy centered around 2 eV, allows us to eliminate these contributions [Fig. 3(c) and (d)], indicating that the satellite peaks and the tails are artefacts, due to secondary ions with an anomalous kinetic energy. As mentioned in the introduction, the same kind of phenomenon has been observed with PS [18] and with more complex copolymers [12] for secondary ions above $m/z = 100$.

The lower mass resolution obtained with the energy slit is due to the fact that the secondary optics voltages must be tuned in order to bring the crossover of the secondary ion beam at the exact position of the

slit. By this way, the two-dimensional image transferred by the secondary ion microscope is theoretically reduced to one single point and the secondary ions are selected solely as a function of their kinetic energy. Consequently, the mass resolution is no longer optimized. However, this tuning allows a much more accurate calibration of the mass spectrum, because it is not hampered by the energy dispersion anymore.

To understand the origin of the satellite peaks in the PIB and PBD spectra, the KEDs of the secondary ions were measured. Fig. 4 shows the energy spectra of several unsaturated ions sputtered from the cast PIB layer. The main peak of these distributions, corresponding to ions sputtered from the sample surface, is narrow and intense. In addition, instead of a quick fall of intensity below 0 eV, a significant fraction of ions is detected with a kinetic energy deficit ("negative" part of the distribution). Following the cases, one can see a pattern with one or two well-defined peaks in the negative apparent energy tail. As described in [12,18], these peaks correspond to ions formed by the metastable decay of their parents in the field-free drift region of the spectrometer and the mass of the lost neutral can be determined with

$$\frac{\Delta m}{m}\frac{E_k}{\Delta E_k} = 1 \qquad (12)$$

From this equation, one finds that the more intense peak in the "negative energy" part of the distributions displayed in Fig. 4 is related to daughter ions formed by the loss of H_2 from their metastable parents. The theoretical energy deficit is indicated by vertical bars in Fig. 4. The additional contribution observed in the energy spectrum of $C_3H_3^+$ (m/z = 39) and $C_5H_5^+$ (m/z = 65) is due to a single H loss reaction. Identical reactions are evidenced with PBD samples, too. The main metastable decay reactions affecting PIB and PBD secondary ions are listed in Table 1. They are thus qualitatively similar to those reported for PS [18], except that single H loss reactions are predominent in the case of PS, while H_2 loss prevails for PIB and PBD. It must be noticed that, in these

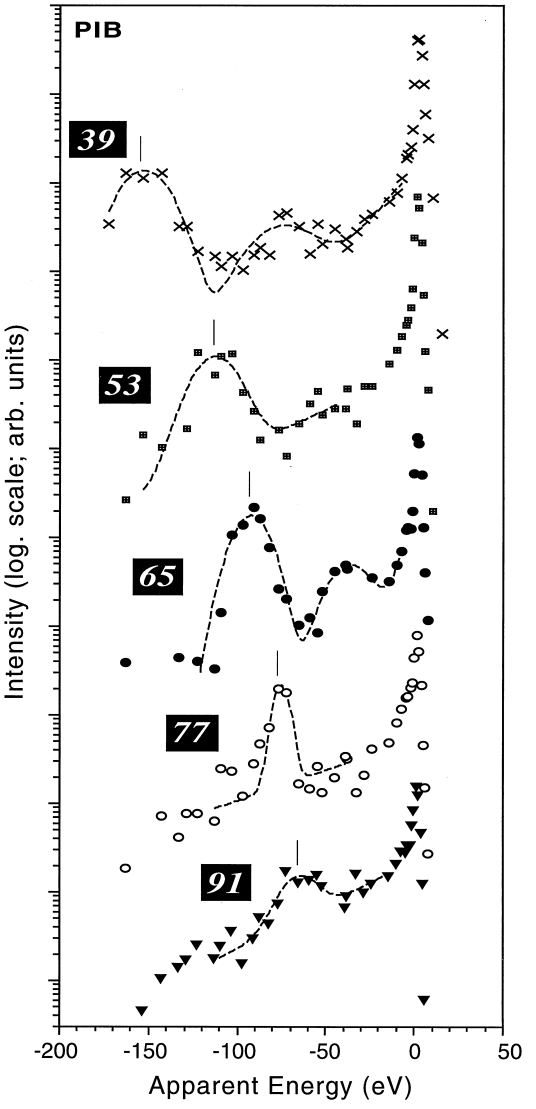

Fig. 4. Kinetic energy distribution of several unsaturated secondary ions sputtered from PIB.

reactions, even electron parents decay by H_2 loss, producing even electron daughters, whereas odd electron parents decay by single H loss, leading to even electron daughters too, in agreement with the even electron rule.

The KEDs indicate that the satellite peaks in the mass spectrum at m/z = 53, 65, 77 [Fig. 3(a)] and 79 are due to these hydrogen loss reactions. In Fig. 5, the intensity of the satellite peak has been integrated

Table 1
Metastable decay reactions for molecular ions sputtered from PIB and PBD

Metastable decay reactions	PIB	PBD
$C_3H_5^+ \rightarrow C_3H_3^+ + H_2$	+	
$C_3H_4^+ \rightarrow C_3H_3^+ + H$	+	+
$C_3H_7^+ \rightarrow C_3H_5^+ + H_2$	+	
$C_4H_7^+ \rightarrow C_4H_5^+ + H_2$	+	
$C_4H_6^+ \rightarrow C_4H_5^+ + H$		+
$C_5H_7^+ \rightarrow C_5H_5^+ + H_2$	+	+
$C_5H_6^+ \rightarrow C_5H_5^+ + H$	+	+
$C_5H_8^+ \rightarrow C_5H_7^+ + H$		+
$C_6H_7^+ \rightarrow C_6H_5^+ + H_2$	+	+
$C_6H_6^+ \rightarrow C_6H_5^+ + H$		+
$C_6H_9^+ \rightarrow C_6H_7^+ + H_2$	+	+
$C_6H_8^+ \rightarrow C_6H_7^+ + H$	+	+
$C_7H_9^+ \rightarrow C_7H_7^+ + H_2$	+	+
$C_7H_8^+ \rightarrow C_7H_7^+ + H$		+
$C_7H_{11}^+ \rightarrow C_7H_9^+ + H_2$	+	+
$C_8H_9^+ \rightarrow C_8H_7^+ + H_2$		+
$C_8H_{11}^+ \rightarrow C_8H_9^+ + H_2$		+

and normalized by the main peak intensity for $C_5H_5^+$ ($m/z = 65$) and $C_6H_5^+$ ($m/z = 77$) sputtered from PIB samples with different coverages. It is striking to see that the daughter fraction is nearly constant whatever the substrate coverage. Fig. 5 suggests that the internal energy distribution of the parents is similar with or without the influence of the substrate,

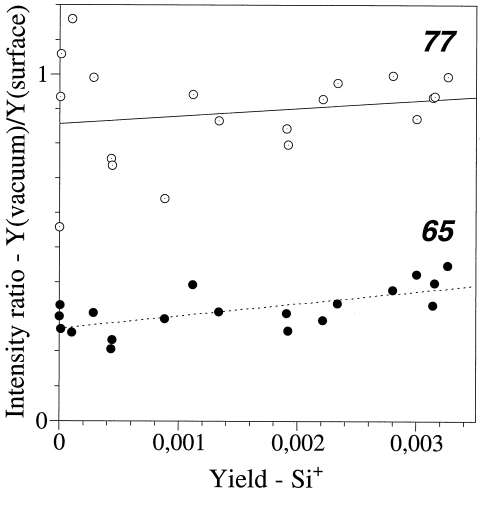

Fig. 5. Ratio of the *number of ions in the satellite peak per ion in the main peak* as a function of the yield of the substrate ion, Si^+, for dilute PIB solutions cast on silicon.

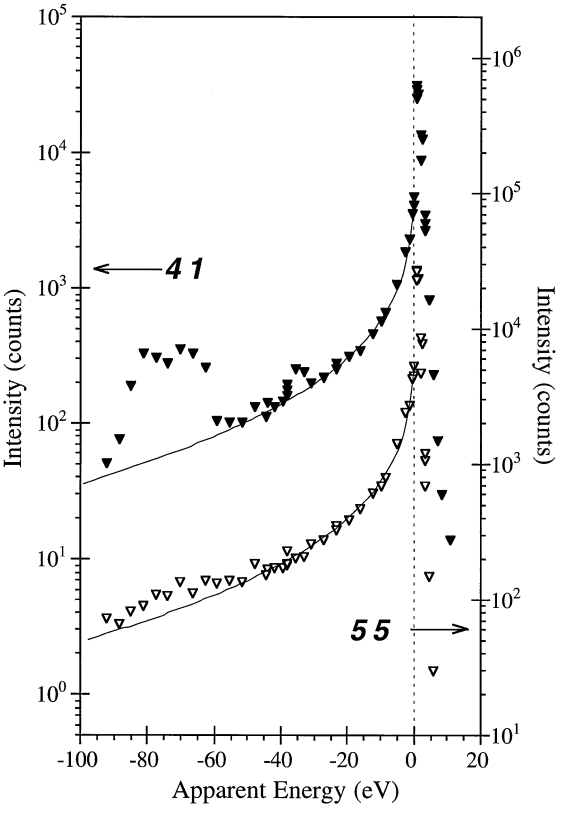

Fig. 6. Kinetic energy distribution of two intense secondary ions sputtered from PIB ($C_3H_5^+$ and $C_4H_7^+$). The negative part of the distribution is fitted by Eq. (6).

although the sputtering and ionisation processes might have been modified.

In most cases, the KEDs do not exhibit well-defined peaks in the negative energy range, but the intensity related to ions with an energy deficit remains significant. This is illustrated in Fig. 6 for $C_4H_7^+$ ($m/z = 55$) sputtered from PIB. The intensity of ions produced in the vacuum decreases regularly with increasing energy deficit. This slow decay is observed for $C_3H_5^+$ ($m/z = 41$), too, with two additional peaks located approximately at -35 and -75 eV. The measurements shown in Fig. 6 were realized with a nominal sample voltage $V = 1500$ instead of 3000. Therefore, according to Eq. (12), the intense peak centered around -75 eV in the KED of $C_3H_5^+$ is due to a H_2 loss reaction from $C_3H_7^+$. The small peak corresponding to -35 eV might be attributed to a

Table 2
Values of the parameter Kr for two molecular ions sputtered from PIB

	Kr [Eq. (6)]	Kr [Eq. (7)]	Decay rate $-$ $r(/s^{-1})$ $1 < \Delta m < 100\ m_d$
$C_3H_5^+$			
[a]$V = 1500$	0.45	0.54	
[b]$V = 3000$	0.26	0.28	$3 \times 10^7 \leq r \leq 2 \times 10^8$
a/b	*1.7*	*1.9*	
$C_4H_7^+$			
[a]$V = 1500$	0.31	0.32	
[b]$V = 3000$	0.20	0.18	$2 \times 10^7 \leq r \leq 1 \times 10^8$
a/b	*1.6*	*1.8*	

single H loss reaction. In fact, the regular decay is due to fast unimolecular dissociation in the acceleration section of the spectrometer [25,26]. Nevertheless, the parents in these reactions cannot be identified because, even with the approximations described in the theoretical section, Eq. (12) must be replaced by

$$\frac{\Delta m}{m}\frac{E_k}{\Delta E_k} = \frac{d}{l_{\text{acc}}} \tag{13}$$

in this part of the spectrometer where d is the distance where the dissociation occurs. In Eq. (13), Δm and d are unknown, and these quantities are then impossible to determine without further information. It is interesting to notice that, in general, the regular decay does not stop after the well-defined peaks (Fig. 4), indicating that the identified reactions are not the cause of this softly decaying baseline. In Fig. 6, the negative energy tails of the KEDs of $C_3H_5^+$ ($m/z = 41$) and $C_4H_7^+$ ($m/z = 55$) were fitted with Eq. (6), according to the hypotheses mentioned in Sec. 3. The fit gives access to the product Kr, proportional to the dissociation rate of the metastable parents. The values of Kr determined by Eq. (6) are indicated in the first column of Table 2 for two different measurements (nominal sample voltage (V) = 1.5 and 3 kV). As r is a constant of the reaction and K is proportional to V^{-1}, the ratio $Kr(V = 1500)/Kr(V = 3000)$ should be equal to 2 (a/b in Table 2). Table 2 shows that the ratios calculated from the fits are slightly lower, but the trend is respected.

To verify these particular values and, in general, the application of our simple model (one single decay reaction with a narrow distribution of internal energy), measurements of the integral of the KED were realized. By moving the edge of the energy slit through the secondary ion beam, it is possible to cut the high energy part of the distributions beyond a given energy E_k. This gives an experimental estimation of the integral calculated in Eq. (7). The results of these measurements are reported in Fig. 7 for $C_3H_5^+$ and $C_4H_7^+$ and for two values of the nominal sample voltage. The integrated intensity decrease with increasing energy deficit is faster with a nominal sample voltage of 1500 V because a given energy deficit in Fig. 7 corresponds to a greater fraction of the total kinetic energy of the parent for $V = 1500$ than for $V = 3000$ and to a longer time spent in the acceleration section when dissociation occurs. The best fits with Eq. (7) are indicated by full lines in Fig. 7. The agreement with the data is very good in all cases. The characteristic values of the parameter Kr corresponding to the different curves in Fig. 7 are listed in Table 2, column 2. First, these values are reasonably close to those obtained from the usual KED measurements (first column), which is a first confirmation and gives an estimation of their accuracy. Second, the ratios $Kr(V = 1500)/Kr(V = 3000)$ (a/b) in column 2 are closer to 2, and the equation used for the fit is simpler, which might indicate that the results derived from the integral KED measurements are closer to reality. Similar conclusions can be drawn from the detailed analysis of the KED measurements for all the tested secondary ions, i.e. for the intense C_xH_y ions below $m/z = 200$.

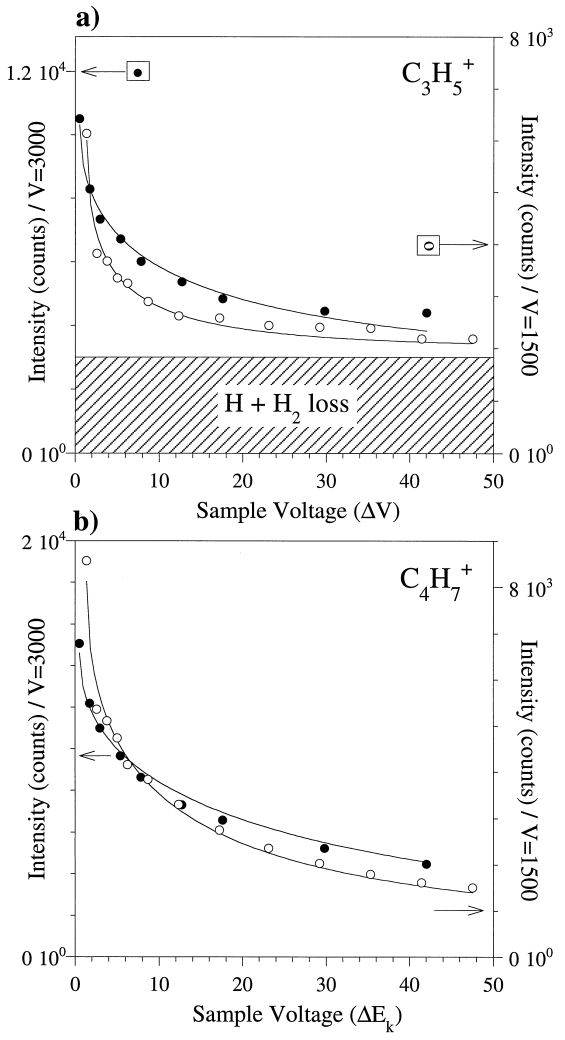

Fig. 7. Integral of the negative part of the distributions of $C_3H_5^+$ and $C_4H_7^+$, up to the energy deficit ΔE_k, for two nominal sample voltages, 1500 and 3000 V.

In Fig. 7(a), the results were scaled to display the intensity fraction corresponding to the identified H and H_2 loss reactions occuring in the field-free drift region. As the metastable decay times for these reactions are much longer (see Sec. 4.4), the integrated intensity decrease due to metastable decay in the acceleration section should tend asymptotically to the intensity due to decay in the drift region. Indeed, the curves in Fig. 7(a) tend to a threshold which is close to the intensity measured for H and H_2 loss

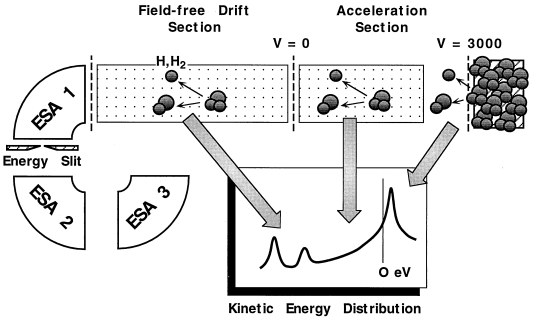

Scheme 1. Dissociation channels evidenced for molecular ions sputtered from hydrocarbon polymers (PIB, PBD, PS) and their relation with the KED. In order of increasing distance from the surface (decreasing internal energy): fragmentation in the surface region, dissociation in the acceleration section, H and H_2 loss in the field free drift section.

reactions in the field free drift region. Moreover, this suggests that H and H_2 losses are the only reactions contributing significantly to the production of $C_3H_5^+$ in the drift region of the spectrometer. For $C_4H_7^+$ [Fig. 7(b)], the existence of a threshold is not evident, which is in agreement with the absence of well-defined peaks in the negative energy tail of this ion KED in Fig. 6.

To summarize this section, the different fragmentation channels evidenced for hydrocarbon molecular ions are described in Scheme 1: (1) direct fragmentation at the surface, corresponding to the main peak of the KED; (2) fast metastable decay in the acceleration section of the spectrometer, explaining the regular intensity decrease in the negative energy tail and (3) loss of H and H_2 in the drift region of the spectrometer, leading to additional peaks for quantified energy deficits. These metastable decay reactions can be explained with simple arguments based on the unimolecular reactions theory [14].

4.3. Metastable fractions

The fraction of daughter ions produced in the acceleration and drift sections were determined by integrating the negative energy part of the KEDs for most of the secondary ions sputtered from PIB, PBD, and PS cast on silicon. The results are reported in Figs. 8, 9, and 10 for PIB, PBD, and PS respectively.

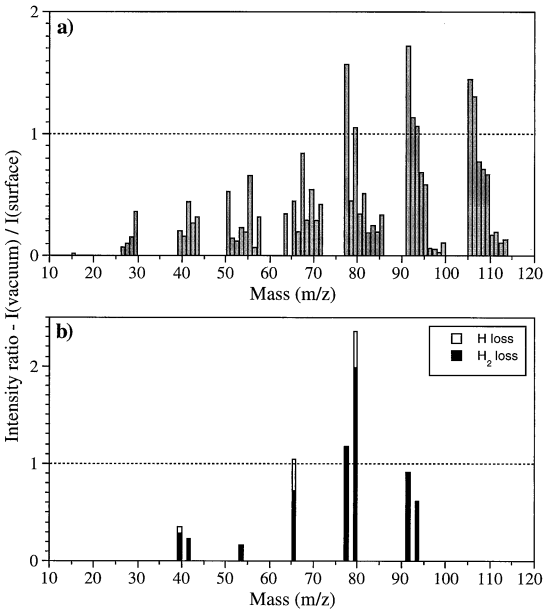

Fig. 8. Ratios of the *number of ions produced in the vacuum per ion produced at the surface* as a function of the daughter ion mass for PIB. (a) Fast metastable decay in the acceleration section. (b) Integrated intensity of the daughter ions resulting from H and H_2 losses.

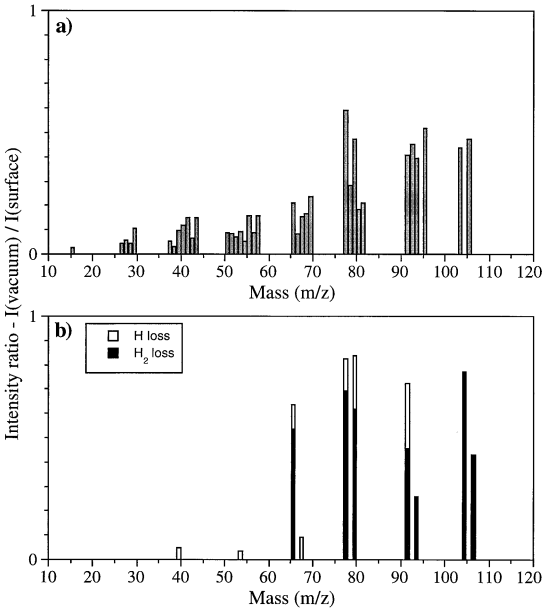

Fig. 9. Ratios of the *number of ions produced in the vacuum per ion produced at the surface* as a function of the daughter ion mass for PBD. (a) Fast metastable decay in the acceleration section. (b) Integrated intensity of the daughter ions resulting from H and H_2 losses.

For each secondary ion, the *Y* axis indicates the ratio of the number of ions produced in the vacuum per ion produced at the surface. Parts (a) and (b) of these figures correspond, respectively, to the metastable decay in the acceleration section (a) and in the drift region (b).

Several observations can be drawn from these figures. In all cases, both reactions in the acceleration section (a) and in the drift region (b) are important ion formation channels.

Concerning the reactions observed in the acceleration section [Figs. 8(a), 9(a), and 10(a)].

(1) On average, the fraction of ions produced by fast metastable decay increases with the mass of the daughter ion. This cannot be explained by the fact that heavy parents spend a longer time in the acceleration section than lighter ones. Indeed, the reactions observed in the acceleration section are so fast that they occur completely in this section, for fast small ions as well as for slower heavy ions. The same trend has been reported by Zubarev and co-workers for secondary ions sputtered from a peptide mixture under 72 MeV, $^{127}I^{13+}$ ion bombardment [13]. A possible explanation is that small ions, sputtered from the high deposited energy region, have already lost their internal energy excess by direct fragmentation during the emission process. In contrast, larger molecular ions, which are thought to be produced farther from the primary impact point, might be emitted without extensive fragmentation, but with a certain amount of internal energy leading to the delayed decomposition.

(2) The relative importance of the ion production by fast metastable decay follows the order of increasing hydrogen content of the polymers (PIB > PBD > PS).

(3) In the case of PIB, it is clear that the fraction of ions formed in the vacuum is very weak for characteristic ions ($C_4H_8^+$—$m/z = 56$, $C_7H_{13}^+$—$m/z = 97$, $C_7H_{14}^+$—$m/z = 98$, $C_8H_{15}^+$—$m/z = 111$ and $C_8H_{16}^+$—$m/z = 112$). In the contrary, the ratio I(vacuum)/I(surface) is larger than 1 for stable, aro-

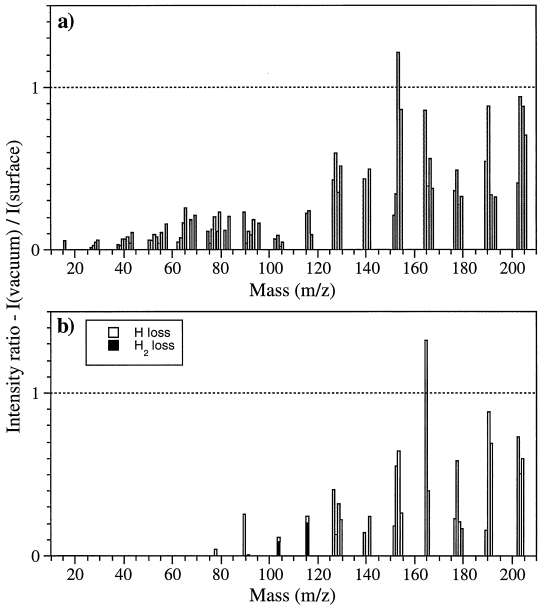

Fig. 10. Ratios of the *number of ions produced in the vacuum per ion produced at the surface* as a function of the daughter ion mass for PS. (a) Fast metastable decay in the acceleration section. (b) Integrated intensity of the daughter ions resulting from H and H_2 losses.

matic secondary ions ($C_6H_5^+$—$m/z = 77$, $C_7H_7^+$—$m/z = 91$, $C_8H_9^+$—$m/z = 105$).

Concerning the reactions observed in the drift region [Figs. 8(b), 9(b), and 10(b)].

(1) Only H and H_2 losses are evidenced and these reactions are sufficient to explain the thresholds in the integral KED measurements [Fig. 7(a)].

(2) The ions produced by these reactions have often an aromatic structure. This is probably due to the particular stability of (poly)cyclic ions. In this respect, it is interesting to note that for unsaturated hydrocarbon polymers, intense molecular ions observed beyond $m/z = 200$ in the mass spectra are (poly)cyclic aromatic ions [32–34]. This is valid for PS, but also for PBD, polyisoprene, etc. These ions do not reflect the polymer chemical structure (even in the case of PS), and their emission needs a complex reorganization of the precursor, involving multiple hydrogen losses. The fact that such large molecular ions may survive to multiple bond breaking without fragmenting into much smaller ions indicates their high stability. This stability must act as a driving force in the metastable decay process, too.

(3) Whereas H_2 loss is predominent for PIB and PBD secondary ions, it is minor for PS. In the case of PS, a single H loss is the main decay channel. For large (poly)cyclic daughter ions produced from PS, this may be explained because the heavy species leaving the surface are already aromatic or very unsaturated. Then, the simultaneous loss of two hydrogen atoms might be less probable, or it would lead to a structure which is no longer cyclic, due to the hydrogen deficit, and thus, less stable.

(4) For PIB and PBD, important fractions of ions formed in the vacuum are observed below $m/z = 100$, while it occurs mostly for heavier ions with PS. Again, the secondary ions emitted from PS are already very unsaturated and stable, which should reduce the probability to decay by hydrogen losses. This explanation might account for the decreasing fraction of metastable decay with increasing polymer unsaturation in the acceleration section, too.

The importance of metastable decay reactions for ions sputtered from hydrocarbon polymers can be summarized by the total metastable fraction, which is equal to 26% for PIB, 15% for PBD and 15% for PS.

4.4. Decay rates

For the unimolecular dissociation reactions occurring in the drift region of the spectrometer, the decay rates can be calculated assuming the hypotheses described in Sec. 3 (one single reaction per parent; very narrow distribution of internal energy for the parent). In that frame, Eq. (11) is valid and r can be calculated knowing Y_p^{det} and Y_d^{drift}. In practice, these two values are obtained from the integration of the different peaks of the KEDs. The calculated decay rates (r) are reported in Table 3 for the three polymer samples. Most of them are in the range 10^4–10^5 s^{-1}, except for some PS ions. The corresponding half lives [$\tau_{1/2} = \ln(2)/r$] are then in the range 10–100 μs. For comparison purpose, these decay rates correspond respectively to 7–8 and 8–9 eV internal energies for the metastable loss of H from naphtalene and phenanthrene [36]. Similar half lives have been measured for

Table 3
Calculated decay rates for the H and H_2 loss reactions (10^4 s^{-1})

Daughter ion mass (m/z)	*PIB*		*PBD*		*PS*	
	H loss	H_2 loss	H loss	H_2 loss	H loss	H_2 loss
39	3.8	1.5	3.2			
41		2.6				
65		1.6	1.6			
77		3.9	1.8	3.2	1.2	
79	3.8	2.7	3.3	3.4		
91		3.7	5.1	4.2	0.8	
93		1.2		2.3		
103				1.8	0.4	0.8
128					2.1	
152					3.1	
165					2.6	
178					1.8	

the loss of one repeat unit in perfluorinated polyethers fragments [19], for the decay of various parentlike ions of phenylalanine [11] and for $(CsI)_nCs^+$ clusters [22]. On the other hand, the half lives measured for protonated valine molecules and dimers loosing respectively a CH_2O_2 and a molecule were shorter ($\sim$1 μs) [20].

As mentioned in Sec. 3, it is impossible to determine decay rates for ions dissociating in the acceleration section, because both t and Δm are unknown in Eq. (4). Nevertheless, knowing the value of the parameter Kr (Table 2) and the definition of K [Eq. (5)], it is possible to draw r versus Δm curves for each secondary ion (not shown). In these curves, r increases quickly with increasing Δm, goes through a maximum for $\Delta m = m/2$, i.e. when the mass of the lost neutral is equal to the mass of the daughter ion, and decreases slowly beyond the maximum. In the case of $C_3H_5^+$ and $C_4H_7^+$, the lower and upper values of r are given in Table 2, for $1 \leq \Delta m \leq 100\ m_d$, which probably accounts for the real situation. The obtained decay rates are in the range 10^7–10^8 s^{-1}, corresponding to half lives of 10–100 ns, which is much faster than the H and H_2 loss reactions observed in the drift region of the spectrometer. Similar decay rates have been observed by Dzhemilev and coworkers for metal clusters (Ta_n^+ [25], Nb_n^+ and Fe_n^+ [26]) losing an atom. Even shorter lifetimes were predicted by Wucher and Garrison for sputtered Ag_n^+ clusters [37].

5. Conclusions

The KED measurements show that unimolecular dissociation processes play an important role in SIMS of hydrocarbon polymers. An important fraction of the secondary ions observed in the fingerprint region of the polyisobutylene (26%), polybutadiene (15%) and polystyrene (15%) SI mass spectra is formed in the vacuum, by the decomposition of larger parent ions. Two kinds of reactions are evidenced: (1) fast metastable decay in the acceleration section of the spectrometer, corresponding to half lives of 10 ns to 0.1 μs; (2) delayed H and H_2 losses in the drift section of the spectrometer, corresponding to half lives of 10–100 μs.

The integrated daughter ion intensities indicate that, on average, the fraction of ions produced by fast metastable decay increase with the ion mass, at least in the region $0 < m/z < 200$. Concerning the decay in the drift section of the spectrometer, H_2 loss is the main decay channel for ions sputtered from polyisobutylene and polybutadiene, whereas single H loss prevails for (poly)aromatic hydrocarbon ions sputtered from polystyrene.

To get more information about the details of the processes (decay rates, etc), the data were interpreted on the basis of the unimolecular reactions theory, with the following hypotheses: the metastable parents decompose mainly via one major reaction in the drift section (H or H_2 loss); the internal energy distributions are narrow, and centered around a value E_{int} corresponding to a given rate r. The good fit of the negative energy tails of the KEDs validates the second hypothesis and suggests that each daughter is produced by one major reaction in the case of fast metastable decay reactions. On the other hand, the integral KED measurements indicate that there is no need to invoke other reactions than H and H_2 losses in the drift section to account for the intensity thresholds observed in the acceleration section.

Acknowledgements

The authors wish to thank Pr. R. Jérôme at University of Liège for providing the PS beads. Dr. B.G. Segda is acknowledged for his contribution to the measurements and data processing. We are also grateful to Dr. B.W. Schueler for his comments concerning the interpretation of the results. This work and A. Delcorte are supported by the "Action de Recherche Concertée" (94/99-173) of the "Communauté Française de Belgique, Direction Générale de l'Enseignement Supérieur et de la Recherche Scientifique." The TOF-SIMS equipment was acquired with the support of the "Région Wallonne" and "FRFC-Loterie Nationale" of Belgium.

References

[1] A. Benninghoven, F.G. Rüdenauer, H.W. Werner, Secondary Ion Mass Spectrometry, Wiley, New York, 1987, p. 699.
[2] P. Bertrand, L.-T. Weng, Mikrochim. Acta (Suppl.) 13 (1996) 167.
[3] G.J. Leggett, in Wiley Static SIMS Library, J.C. Vickerman, D. Briggs, A. Henderson (Eds.), Wiley, New York, 1996, p. 19.
[4] P.A. Demirev, Mass Spectrom. Rev. 14 (1995) 279.
[5] H.M. Urbassek, Nucl. Instrum. Methods B 18 (1987) 587.
[6] R. Hoogerbrugge, P.G. Kistemaker, Nucl. Instrum. Methods B 21 (1987) 37.
[7] A. Benninghoven, in Ion Formation from Organic Solids, Springer Series in Chemical Physics 25, A. Benninghoven (Ed.), Springer-Verlag, Berlin, 1983, p. 77.
[8] R.S. Taylor, B.J. Garrison, Langmuir 11 (1995) 1220.
[9] P. Bertrand, A. Delcorte, SIMS XI Proceedings, R. Lareau, G. Gillen (Eds.), Wiley, New York, 1998, p. 437.
[10] R.M. Papaléo, G. Brinkmalm, D. Fenyö, J. Eriksson, H.-F. Kammer, P. Demirev, P. Hakansson, B.U.R. Sundqvist, Nucl. Instrum. Methods B 91 (1994) 667.
[11] B. Schueler, R. Beavis, W. Ens, D.E. Main, X. Tang, K.G. Standing, Int. J. Mass Spectrom. Ion Processes 92 (1989) 185.
[12] A. Delcorte, P. Bertrand, SIMS XI Proceedings, R. Lareau, G. Gillen (Eds.), Wiley, New York, 1998, p. 447.
[13] R.A. Zubarev, U. Abeywarna, P. Hakansson, P. Demirev, B.U.R. Sundqvist, Rapid Commun. Mass Spectrom. 10 (1996) 1966.
[14] W. Forst, Theory of Unimolecular Reactions, Academic, New York, 1973.
[15] K.G. Standing, W. Ens, R. Beavis, in Ion Formation from Organic Solids, Springer Series in Chemical Physics 25, A. Benninghoven (Ed.), Springer-Verlag, Berlin, 1983, p. 107.
[16] X. Tang, W. Ens, N. Poppe-Schriemer, K.G. Standing, in Methods and Mechanisms for Producing Ions from Large Molecules, K.G. Standing and W. Ens (Eds.), Plenum, New York, 1991, p. 139.
[17] G. Gillen, Int. J. Mass Spectrom. Ion Processes 105 (1991) 215.
[18] A. Delcorte, B.G. Segda, P. Bertrand, Surf. Sci. 381 (1997) 18; A. Delcorte, B.G. Segda, P. Bertrand, ibid. 389 (1997) 393.
[19] H. Feld, A. Leute, D. Rading, A. Benninghoven, M.P. Chiarelli, D.M. Hercules, Anal. Chem. 65 (1993) 1947.
[20] D.F. Barofsky, G. Brinkmalm, P. Hakansson, B.U.R. Sundqvist, Int. J. Mass Spectrom. Ion Processes 131 (1994) 283.
[21] R.A. Zubarev, Ph.D. thesis, Uppsala, 1997.
[22] B. Schueler, R. Beavis, G. Bolbach, W. Ens, D.E. Main, K.G. Standing, SIMS V, Springer Ser. Chem. Phys. 44 (1986) 57.
[23] H.M. Urbassek, W.O. Hoffer, in Fundamental Processes in Sputtering of Atoms and Molecules, P. Sigmund (Ed.), Mat. Phys. Medd., Copenhagen, 1993, Vol. 43, p. 97.
[24] W. Begemann, K.H. Meiwes-Broer, H.O. Lutz, Phys. Rev. Lett. 56 (1986) 2248.
[25] N.K. Dzhemilev, A.M. Goldenberg, I.V. Veryovkin, S.V. Verkhoturov, Nucl. Instrum. Methods B 114 (1996) 245.
[26] A.D. Bekkerman, N.K. Dzhemilev, S.V. Verkhoturov, I.V. Veryovkin, A. Adriaens, EMAS'97 Proceedings, Mikrochim. Acta, Suppl. 15 (1998) 371.
[27] A. Delcorte, P. Bertrand, Surf. Sci. 412/413 (1998) 97.
[28] A. Delcorte, P. Bertrand, Nucl. Instrum. Methods B 135 (1998) 430.
[29] B.W. Schueler, Microsc. Microanal. Microstruct. 3 (1992) 119.
[30] A. Delcorte, L.T. Weng, P. Bertrand, Nucl. Instrum. Methods B 100 (1995) 213.
[31] B.W. Schueler, private communication.

[32] W.J. Van Ooij, R.H.G. Brinkhuis, Surf. Interface Anal. 11 (1988) 430.
[33] D. Briggs, Surf. Interface Anal. 15 (1990) 734.
[34] L.T. Weng, P. Bertrand, W. Lauer, R. Zimmer, S. Busetti, Surf. Interface Anal. 23 (1995) 879.
[35] X. Vanden Eynde, P. Bertrand, R. Jérôme, Macromolecules 30 (1997) 6407.
[36] Y. Gotkis, M. Oleinikova, M. Naor, C. Lifshitz, J. Phys. Chem 97 (1993) 12282.
[37] A. Wucher, B.J. Garrison, Phys. Rev. B 46 (1992) 4885.